SUPPLEMENTARY DATA

UPF1 helicase orchestrates mutually exclusive interactions with the SMG6 endonuclease and UPF2

Lukas M. Langer*, Katharina Kurscheidt, Jerome Basquin, Fabien Bonneau, Iuliia Iermak, Claire Basquin and Elena Conti*

Department of Structural Cell Biology, Max Planck Institute of Biochemistry, Martinsried/Munich, D82152, Germany
* To whom correspondence should be addressed. Tel: +49 89 8578-3606; Fax: +49 89 8578-3605; Email: conti@biochem.mpg.de
Correspondence may also be addressed to Lukas M. Langer. Email: lulanger@biochem.mpg.de

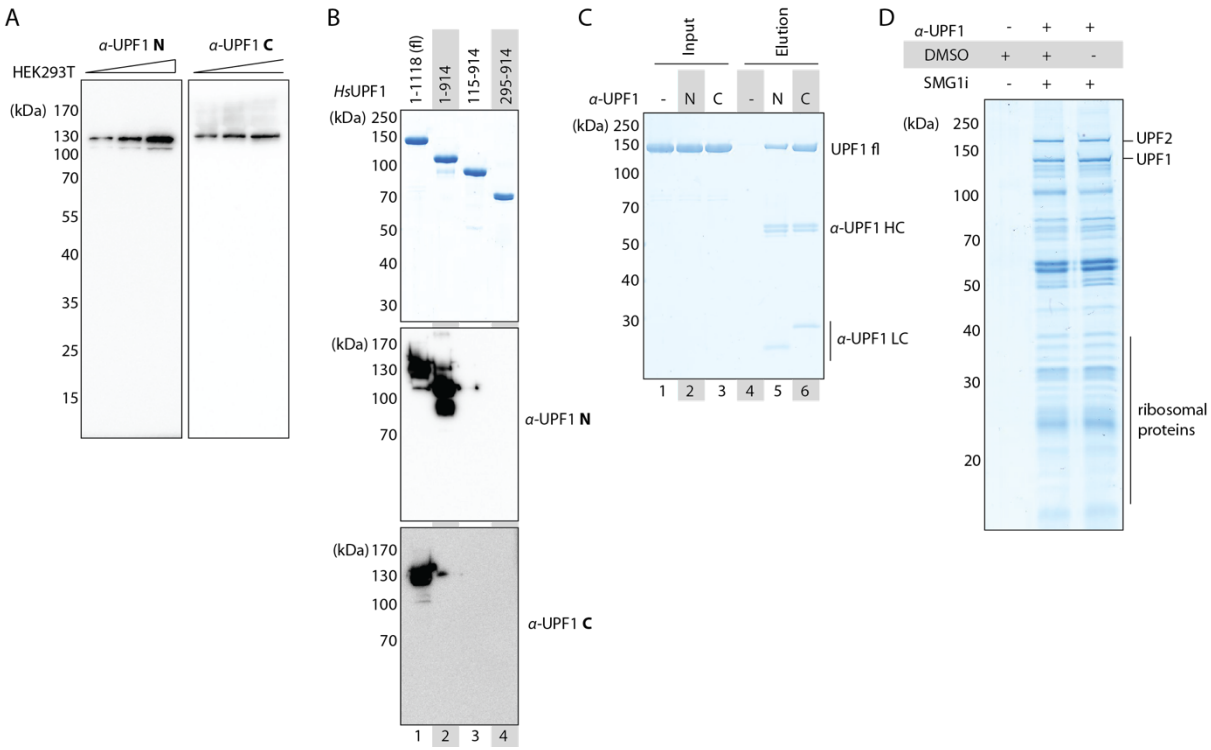

Figure 1 Supplement 1. Characterization of antibodies used for purification of UPF1 mRNPs. (**A**) Immunoblot using either UPF1 antibody against increasing amounts of HEK293T cell lysate. (**B**) Immunoblot using UPF1 antibody N or C against different purified human UPF1 constructs to map the epitope-carrying region for each antibody. (**C**) SDS-PAGE followed by Coomassie-staining and immunoblotting to analyze a pull-down of HEK293T purified full-length human UPF1 using antibody N or C bound to magnetic protein G - coupled beads. (**D**) Coomassie-stained SDS-PAGE showing the protein content pulled down from K562 cell lysate using antibody N bound to magnetic protein G - coupled beads.

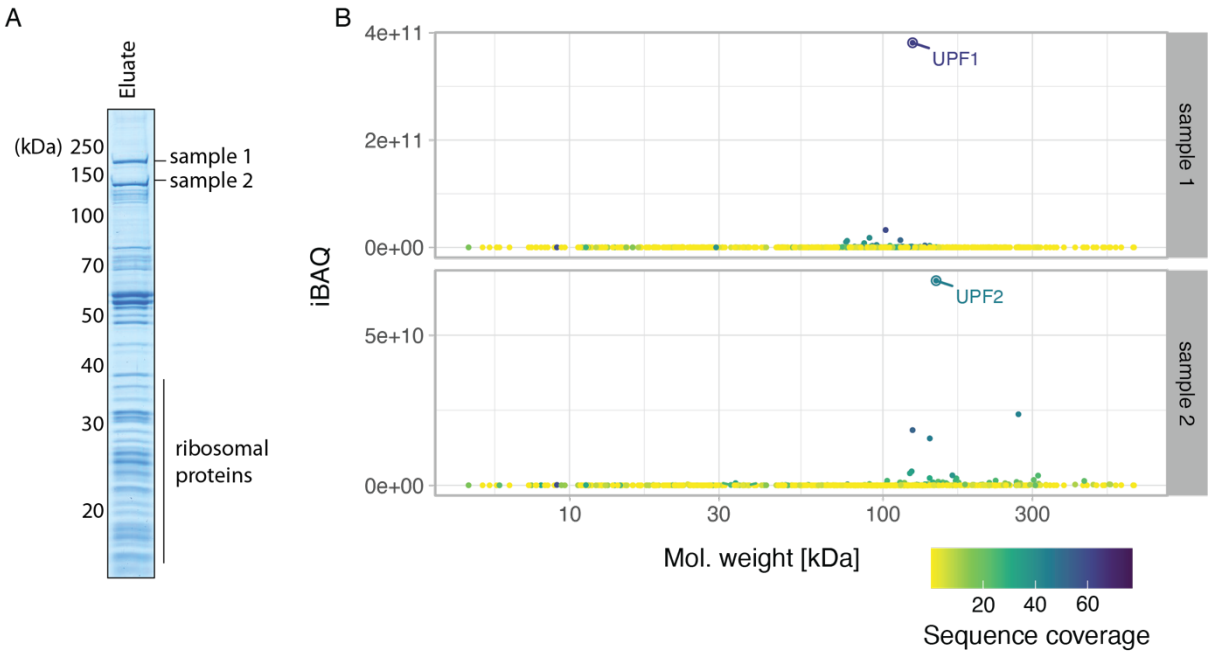

Figure 1 Supplement 2. Peptide mass fingerprinting of selected bands after SDS-PAGE analysis of UPF1 mRNP purifications. (**A**) Coomassie-stained SDS-PAGE with analyzed bands and ribosomal proteins indicated. Gel is the same as shown in Figure 1 B. (**B**) Intensity-based absolute quantitation of proteins identified in selected and cut out gel regions as indicated in panel A. iBAQ values are plotted against the theoretical molecular weight and each dot was colored according to sequence coverage of all detected peptides attributed to this protein.

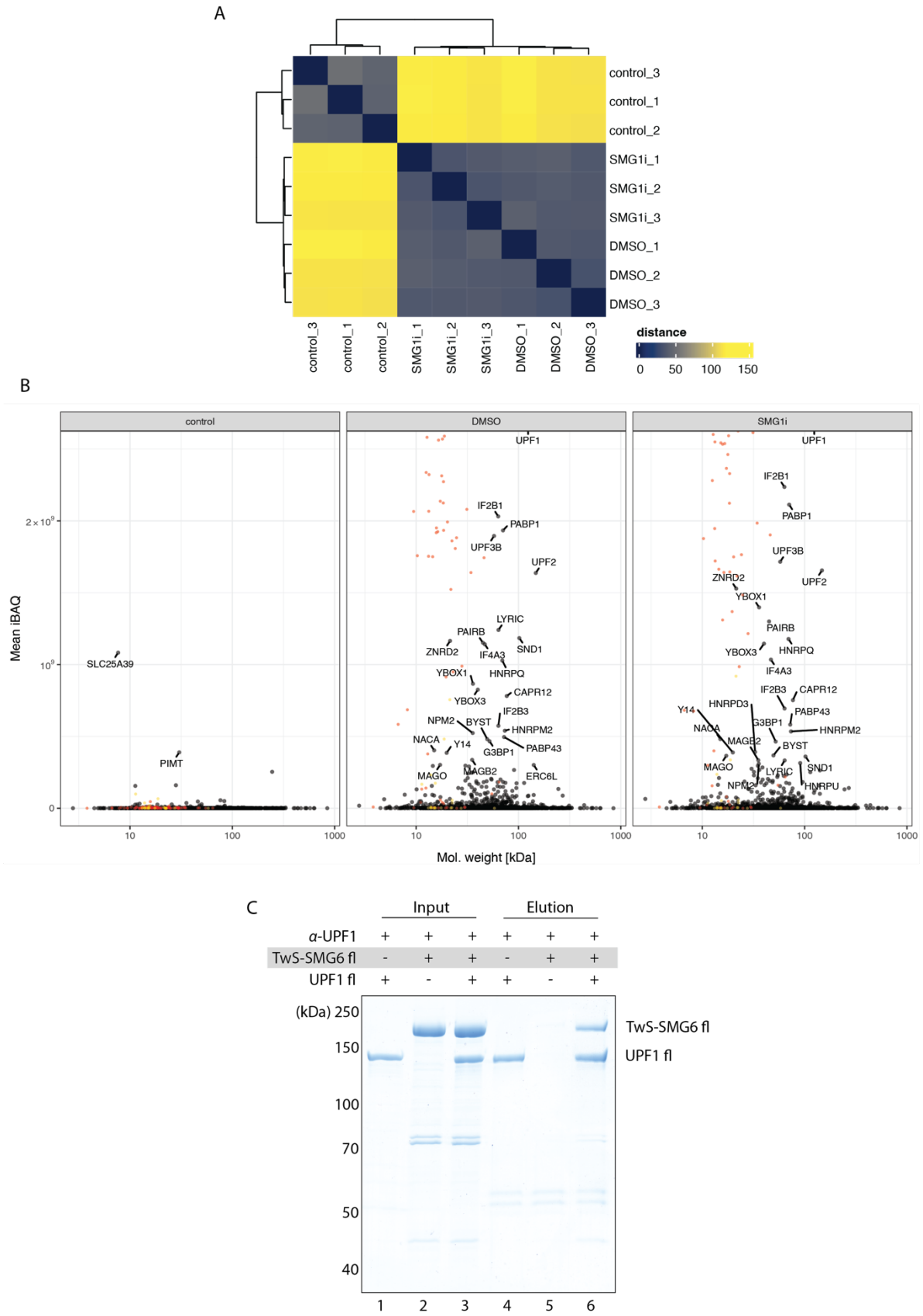

Figure 1 Supplement 3. Characterization of UPF1 mRNPs pulled from K562 lysate. (**A**) Heatmap showing consistency within the three replicates of the three different experimental conditions. Results for pull-downs from DMSO-treated K562 lysate without antibody

(control), with UPF1 antibody N (DMSO) or from SMG1i-treated K562 lysate with UPF1 antibody N (compare Fig. 1 C). (**B**) Mean intensity-based absolute quantitation (iBAQ) values from three conditions with three replicates as in panel A (same experiment), showing the main proteins present in the samples. To highlight non-ribosomal mRNP components, ribosomal proteins are indicated in red but not labeled. Histones are in yellow. (**C**) Coomassie-stained SDS-PAGE of a UPF1 antibody N mediated pull-down of purified full-length human UPF1 and full-length SMG6 wildtype proteins. Input samples are shown in lanes 1 to 3 and SDS-elutions in lanes 4 to 6.

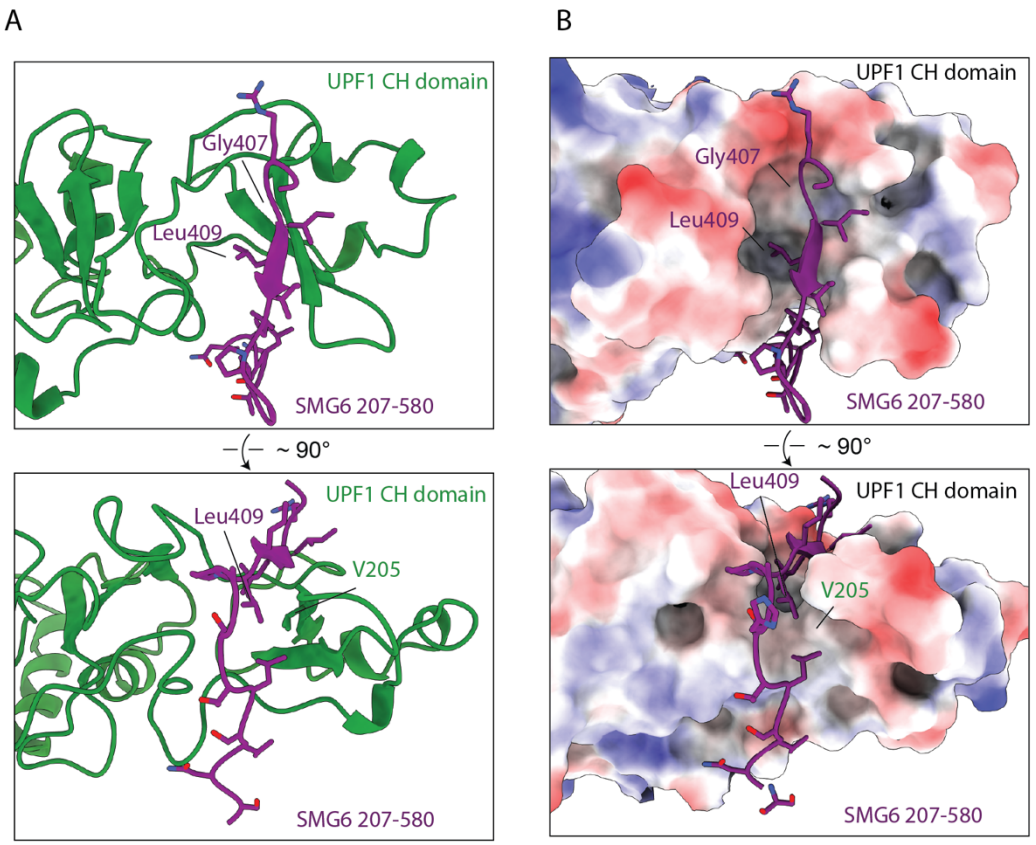
A
B
UPF1 CH domain
Gly407
Leu409
SMG6 207-580
~ 90°
UPF1 CH domain
Leu409
V205
SMG6 207-580
UPF1 CH domain
Gly407
Leu409
SMG6 207-580
~ 90°
Leu409
UPF1 CH domain
V205
SMG6 207-580

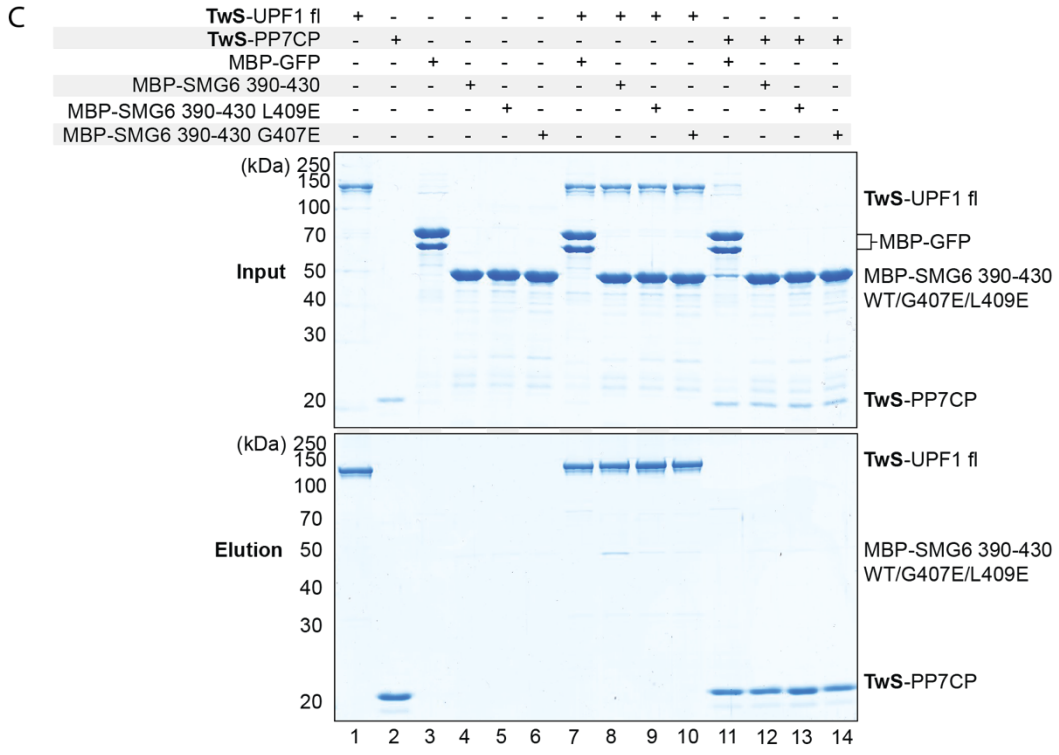
C
TwS-UPF1 fl + - - - - - + + + + - - - -
TwS-PP7CP - + - - - - - - - - + + + +
MBP-GFP - - + - - - + - - - + - - -
MBP-SMG6 390-430 - - - + - - - + - - - + - -
MBP-SMG6 390-430 L409E - - - - + - - - + - - - + -
MBP-SMG6 390-430 G407E - - - - - + - - - + - - - +
(kDa) 250
150
100
70
Input 50
40
30
20
TwS-UPF1 fl
MBP-GFP
MBP-SMG6 390-430
WT/G407E/L409E
TwS-PP7CP
(kDa) 250
150
100
70
Elution 50
40
30
20
TwS-UPF1 fl
MBP-SMG6 390-430
WT/G407E/L409E
TwS-PP7CP
1 2 3 4 5 6 7 8 9 10 11 12 13 14

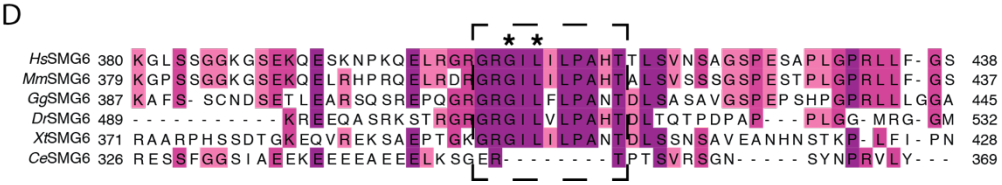
D
HsSMG6 380 KGLSSGGKGSEKQESKNPKQELRGRGRGILILPAHTTLSVNSAGSPESAPLGPRLLF-GS 438
MmSMG6 379 KGPSSGGKGSEKQELRHPRQELRDRGRGILILPAHTALSVSSSGSPESTPLGPRLLF-GS 437
GgSMG6 387 KAFS-SCNDSETLEARSQSREPQGRGRGILFLPANTDLSASAVGSPEPSHPGPRLLLGGA 445
DrSMG6 489 ----------KREEQASRKSTRGRGRGILVLPAHTDLTQTPDPAP---PLGG-MRG-GM 532
XtSMG6 371 RAARPHSSDTGKEQVREKSAEPTGKGRGILILPANTDLSSNSAVEANHNSTKP-LFI-PN 428
CeSMG6 326 RESSFGGSIAEEKEEEEAEEELKSGER--------TPTSVRSGN-----SYNPRVLY--- 369

Figure 2 Supplement 1. A conserved motif in SMG6 binds the UPF1 CH domain. (**A**) Two views of the AF-predicted interaction between UPF1 CH domain and SMG6 with residues mutated in pull-down experiments indicated. (**B**) As (A), but with the CH domain shown in surface representation and colored according to electrostatic potential. (**C**) Coomassie-stained SDS-PAGE analysis of a pull-down experiment using purified human full-length UPF1 and a SMG6 truncation. (**D**) Multiple sequence alignment (run with full-length sequences) displaying conservation of the UPF1-interacting region of SMG6 across species.

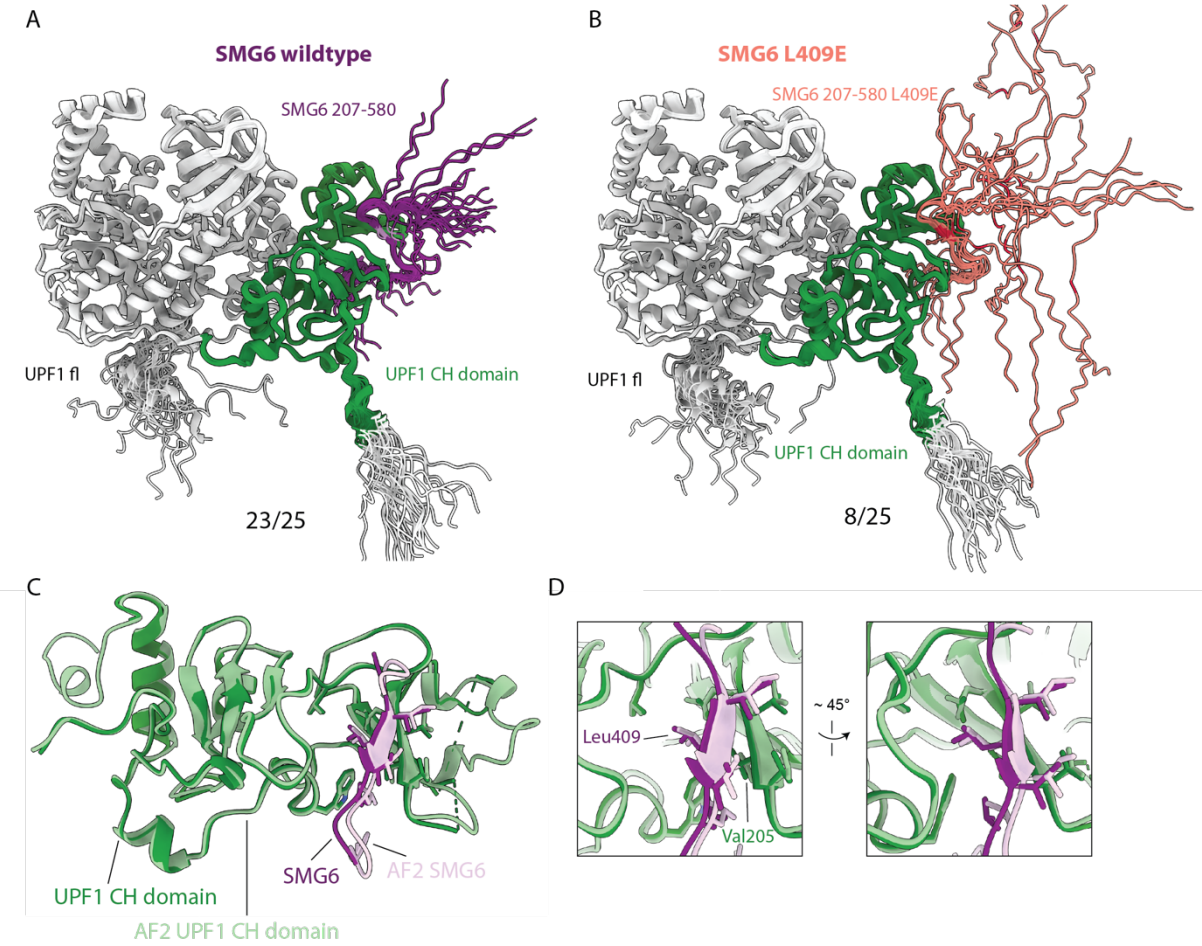

Figure 2 Supplement 2. AlphaFold - Multimer predictions of full-length UPF1 and SMG6 2 07-580 and comparison to X-ray model. (**A**) AlphaFold-Multimer (AF) models of human full-length UPF1 with a region of SMG6 previously identified as interacting (207-580). Unstructured regions are omitted, 23 out of 25 models showed highly similar interaction interfaces. (**B**) As (A), but with a Leu409Glu substitution in SMG6 resulting in only 8 out of 25 models showing highly similar interaction interfaces. (**C**) Superposition of crystal structure and AF prediction of human UPF1 CH domain and SMG6. (**D**) Close-ups highlighting interacting residues in both prediction and experimental data.

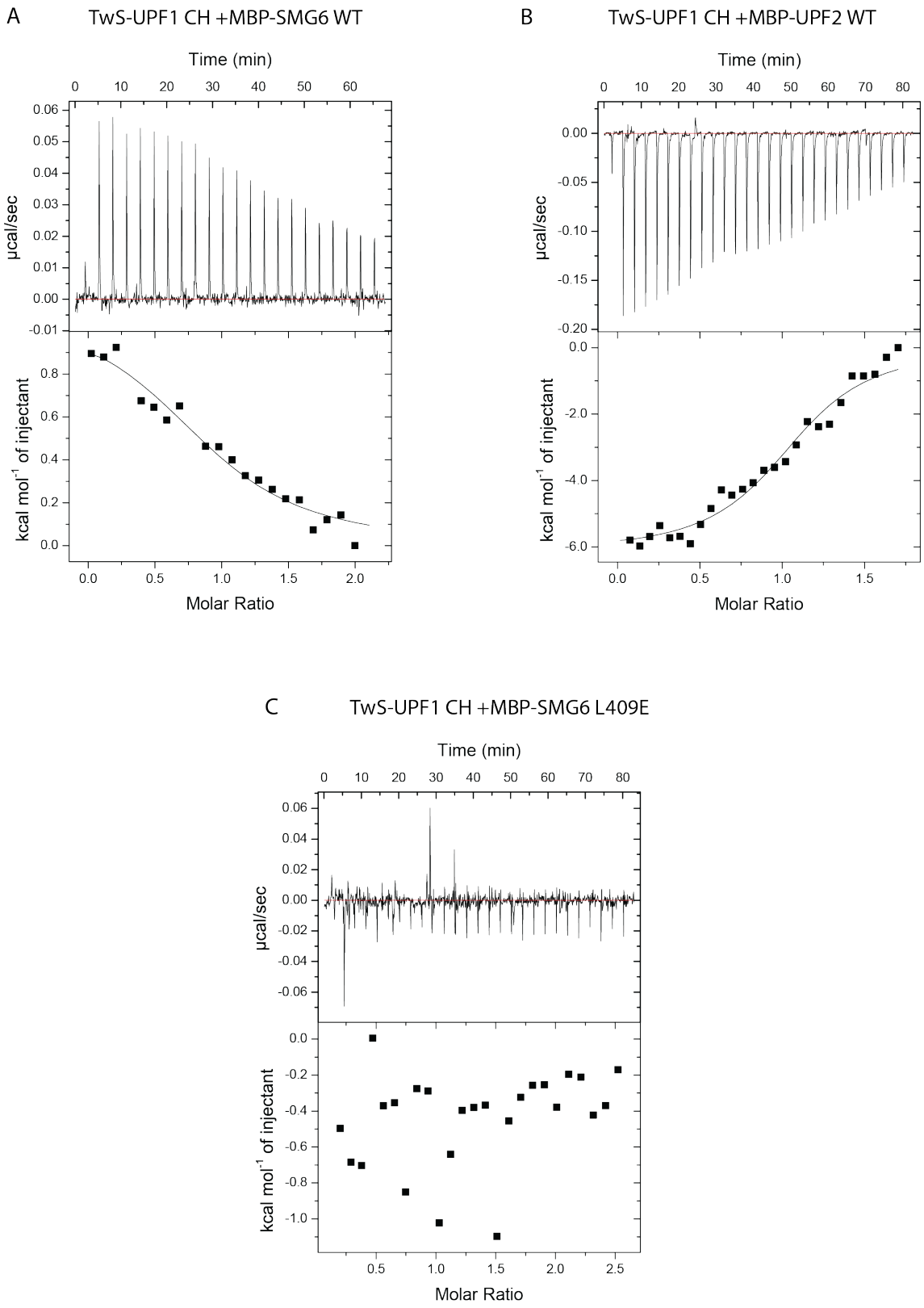

Figure 3 Supplement 1. Calorimetric titration data for the interaction of the UPF1 CH domain with truncations of either SMG6 or UPF2. Isothermal titration calorimetry profiles for the indicated proteins. The shown profiles are representative of at least two

measurements. (**A**) N = 0.95 $^{+}$/$_{-}$ 0.06, K_D = 4.28 $^{+}$/$_{-}$ 0.25 µM; (**B**) N = 1.08 $^{+}$/$_{-}$ 0.02, K_D = 1.46 $^{+}$/$_{-}$ 0.25 µM; (**C**) Data not fitted.

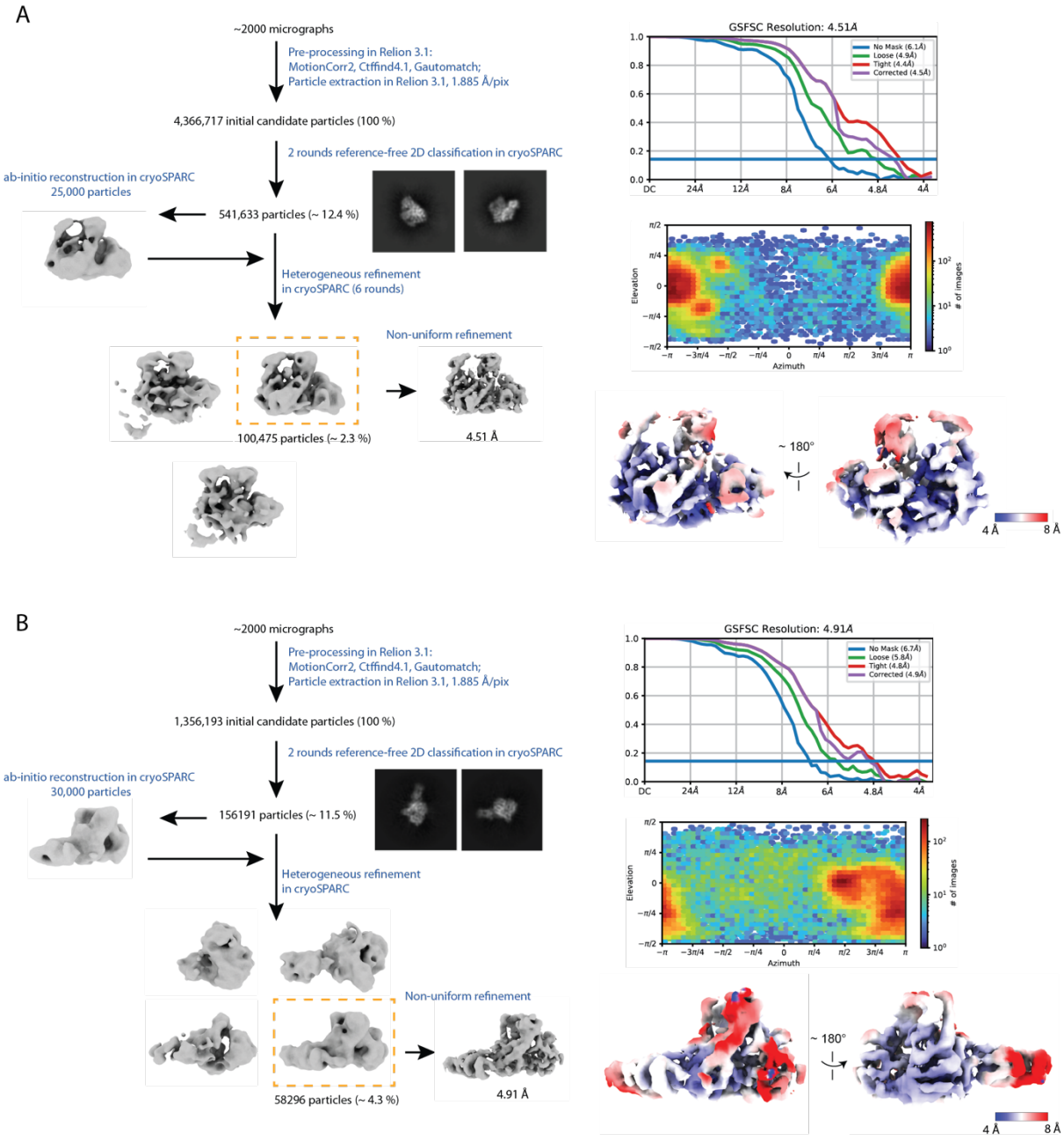

Figure 4 Supplement 1. Cryo-EM processing work-flow and quality assessment for UPF1 data sets. Processing strategy for UPF1 cryo-EM data sets. FSC curves, particle orientation plot and local resolution visualization are included. (**A**) RNA-bound (EMD-19451) and (**B**) RNA-free (EMD-19450).

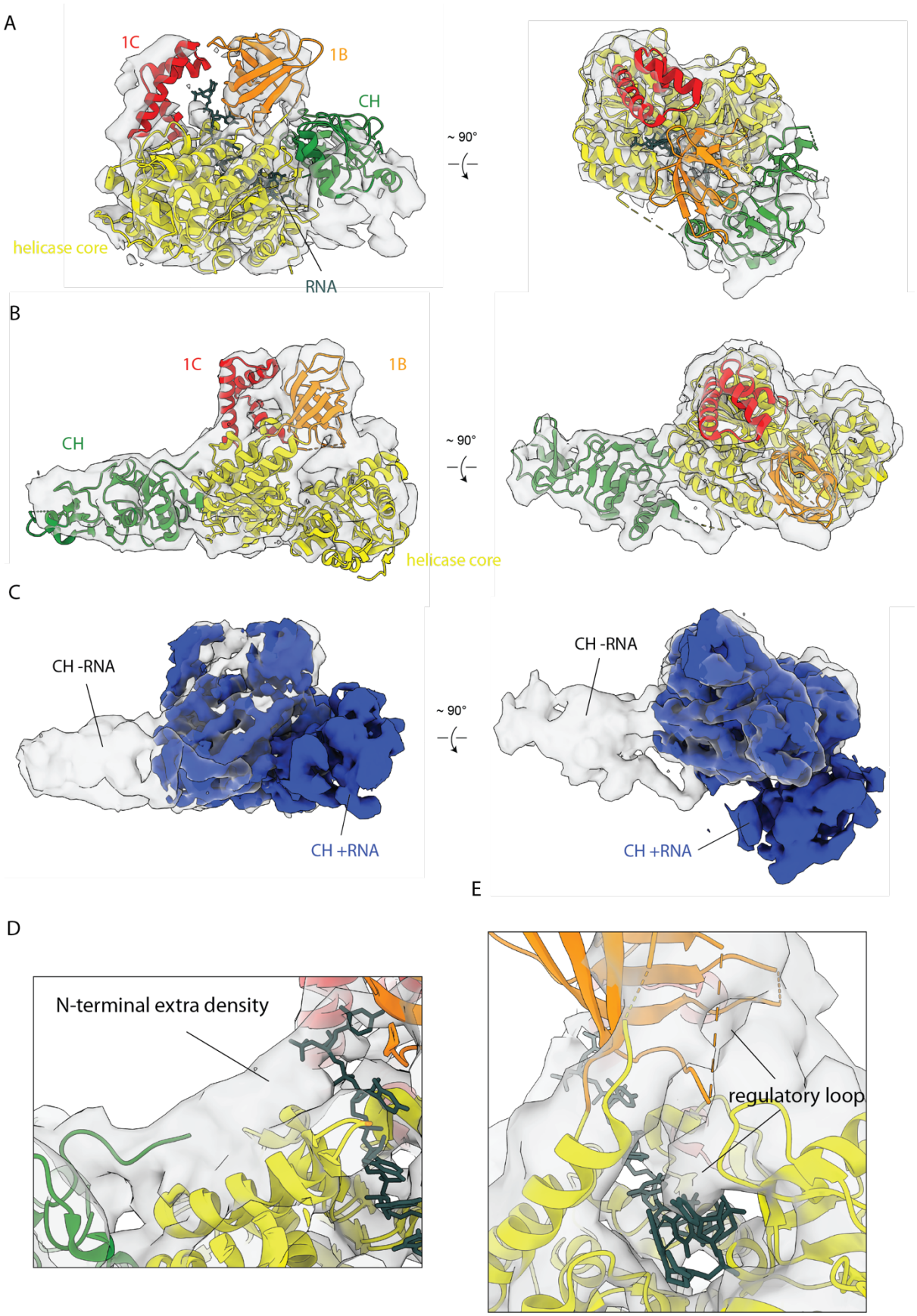

Figure 4 Supplement 2. Details of UPF1 cryo-EM analysis. (**A**) Model of crystallized yeast RNA-bound UPF1 (res. 54-850, PDB: 2XZL) fitted into transparent cryo-EM density

obtained for full-length RNA-bound human UPF1. Note the different relative orientations of the CH domains. A possible explanation are the different ATP analogues used for structure determination (ADP-AlF_4^- in case of the crystal structure and AMP-PNP for cryo-EM). (**B**) Model of crystallized human RNA-free UPF1 (res. 115-914, PDB: 2WJV) fitted into transparent cryo-EM density obtained for full-length human UPF1. (**C**) Density for RNA-bound human UPF1 (blue, compare panel A) fitted into density for RNA-free human UPF1 (transparent grey, compare panel C), visualizing the rearrangement of the CH domain upon RNA binding. (**D**) N-terminal extra density observed in the RNA-free UPF1 data. Density is fitted with both RNA-free and RNA-bound UPF1 models to show how the extra density covers the RNA exit channel. (**E**) RNA-free UPF1 density fitted with yeast RNA-bound model to highlight how the UPF1 regulatory loop obstructs the RNA binding channel in the RNA-free and/or UPF2-bound states.